Airgap Flux-based Estimation of Permanent Magnet Temperature for Thermal Protection of PMSMs

Hyeon-Jun Lee*, Jigyun Jeong*, Marcos Orviz Zapico**, Sang Bin Lee*, David Diaz Reigosa**
and Fernando Briz del Blanco**

* Department of Electrical Engineering,
Korea University,
Seoul, Korea

** Department of Electrical Computer & System Engineering,
University of Oviedo
Gijon, Spain

Abstract—**Airgap flux monitoring has recently received a lot of attention as a low cost means of providing reliable fault detection for permanent magnet synchronous motors (PMSM). In this paper, the feasibility of using an airgap search coil for estimating the temperature of the PM, T_{PM}, for thermal protection is evaluated. Thermal and electrical model- or signal injection-based methods proposed for T_{PM} estimation can provide satisfactory estimates of the average T_{PM} for thermal protection. However, the complexity in the compensation required for non-ideal effects and/or the invasiveness of high frequency signal injection can be limiting factors for implementation. A new method for T_{PM} estimation based on the airgap search coil voltage measurement is proposed in this paper. The proposed method does not require compensation for inverter non-linearity or resistance variation, or injection of high-frequency signals. In addition, it can provide thermal protection based on the T_{PM} estimate of the hottest PM since individual PMs can be monitored. Experimental results on a 2.2 kW IPMSM verify the claims and show that the existing methods can be simplified and enhanced with the proposed method.**

Keywords—*Airgap flux, Interior Permanent Magnet Synchronous Machines, Temperature Estimation, Search Coil, Thermal Protection.*

I. INTRODUCTION

There is a recent trend among low voltage motor manufacturers towards providing self-diagnosis of motors through embedded sensors for reliable operation [1]-[3]. Flux monitoring is being actively investigated as a viable option to complement the conventional thermal, mechanical, and electrical monitoring methods, since it can be implemented with a low-cost search coil [3]-[9]. Airgap flux monitoring is currently being used as an effective means of detecting shorted turns in the rotor field winding in most wound-field synchronous generators with search coils installed on the stator inner surface [8]-[9]. It has recently been shown that airgap flux can provide sensitive indication of anomalies in the magneto-motive force (MMF) and airgap reluctance allowing reliable and sensitive detection of faults in induction and synchronous machines [4]-[7]. It was shown in [10]-[11] that the airgap flux information can also be used to improve the estimate of rotor position for control purposes. Airgap flux monitoring requires installation of a search coil in the motor; but it can be justified for reliability-critical applications if it can provide advanced warning of in-service failures that can lead to catastrophic consequences. The objective of this work is to evaluate the feasibility of using the airgap flux search coil measurement for estimating the temperature of the PM, T_{PM}, for thermal protection in addition to fault detection and control reported in [5]-[7].

NdFeB PMs are a preferred choice for high-performance PMSM drive applications as they provide motors with high efficiency and power density. One of the main concerns in PMSM drive system applications is the degradation in performance and reliability caused by PM demagnetization due to thermal and/or electrical stresses. The residual flux density, B_r, and coercivity, H_c, of PMSMs with NdFeB PMs are known to decrease with PM operating temperature. The increase in PM temperature results in a non-negligible decrease in B_r and H_c with thermal coefficient of $\alpha \approx$ -0.1 %/°C and $\beta \approx$ -0.5 %/°C for B_r and H_c, respectively. Therefore, if the PM is exposed to excessive temperature and/or reverse MMF, this can result in reduced torque production due to reversible or irreversible demagnetization of the PMs [12]-[13]. This shows that monitoring of T_{PM} is critical for both the performance and reliability of the PMSM drive system.

There has been a lot of research activity on estimating T_{PM} indirectly, since direct measurement of the rotating PM with thermal sensors or IR thermography is not practical due to the excessive cost [14]. Most of the recent studies on indirect T_{PM} estimation extract the T_{PM} information from the thermal or electrical model of the PMSM or from the response to an injected high frequency signal [14]-[23]. Each method has advantages and disadvantages in terms of the requirements for implementation, complexity, invasiveness, and performance, as summarized in Table I.

Thermal heat transfer models that represent the heat flow in the motor can be used to estimate T_{PM} from the model and losses in the motor [15]-[16]. This requires the thermal model parameters to be determined from the motor geometry or empirically, and real-time calculation of motor losses, which is a non-trivial task under varying input frequency. One of the disadvantages of using fixed thermal models is that it cannot respond to changes in thermal conditions due to abnormal cooling unless the model parameters are tuned on-line. T_{PM} can also be calculated from the PM flux linkage estimates from the mathematical model of the PMSM [17]-[20]. Although this method requires model parameters and is insensitive in the low-speed range due to low back EMF voltage, it does not require a-priori knowledge of the thermal dynamics within the

PMSM. To overcome the limitations of model and parameter requirements and limited speed range, high-frequency signal injection methods have been proposed in [14], [20]-[24]. It was shown that the d-axis inductance can serve as a robust indicator of T_{PM} over the entire speed range [23]-[24]. However, the additional losses, noise, and vibration produced by the injected high-frequency signal can be a limitation in many applications. In the above-mentioned methods that require electrical variables and parameters for indirect estimation of T_{PM}, non-ideal factors such as the temperature dependency of model parameters, inverter non-linearity, magnetic saturation, and d- and q-axes cross coupling can result in a significant error in the T_{PM} estimate [17]-[27]. Additional measurements, parameters, and/or computation required for compensating for these non-idealities are required for improving the T_{PM} estimation accuracy, and they result in an increase the cost and complexity. Moreover, all indirect methods mentioned above provide the "average" T_{PM} estimate of all PMs, and not the T_{PM} of the "hottest" PM, since the individual PMs cannot be monitored. The relative pros and cons of each T_{PM} estimation approach are summarized in Table I.

The objective of this work is to evaluate if the airgap search coil can be used for thermal protection of the PMs in addition to fault detection and control. A new method of estimating T_{PM} from the search coil measurement is proposed, and experimental verification on a 2.2 kW PMSM is provided to verify the claims made. It is shown that the T_{PM} estimate can be used for thermal protection, and that the existing methods can be significantly simplified and improved. It is also shown that T_{PM} can be estimated independent of R_s and inverter non-linearities, and T_{PM} of the individual PMs can be detected with high sensitivity allowing thermal protection based on the T_{PM} of the hottest PM.

II. PMSM MODEL-BASED ESTIMATION OF PM FLUX LINKAGE FOR PM TEMPERATURE MONITORING

T_{PM} can be directly calculated from the flux linkage of the PM, λ_{PM}, from (1), since the residual flux of the PM decreases with increase in temperature.

$$\lambda_{PM} = \lambda_{PM0}[1 + \alpha \cdot (T_{PM} - T_0)] \qquad (1)$$

In (1), α is the temperature coefficient of the PM material in %/°C, and λ_{PM0} is the value of λ_{PM} at reference temperature, T_0. λ_{PM} can be estimated from the model of the PMSM from the stator voltages and currents, v_{qds} and i_{qds} [17], [20]. The q-axis component of the stator voltage, v_{qs}, in the rotor reference frame is given by

$$v_{qs}^r = R_s i_{qs}^r + p\lambda_{qs}^r + \omega_r \lambda_{ds}^r, \qquad (2)$$

where λ_s and R_s are the stator flux linkage and resistance, and ω_r is the rotor speed. The d-axis stator flux linkage can be expressed as

$$\lambda_{ds}^r = L_{ds}(i_{qs}^r, i_{ds}^r) \cdot i_{ds}^r + \lambda_{PM}^r, \qquad (3)$$

where L_{ds} is the d-axis stator inductance. L_{ds} is represented as a function of i_{qs} and i_{ds} to include the influence of saturation and cross-coupling [13], [26]-[27]. Under *steady state* operation,

Table I. Comparison of different approaches used for PM temperature estimation

	Thermal/ Infrared sensor	Thermal model	Electrical model	Signal injection	Airgap search coil
Additional H/W requirement	−	+	+	+	−
Model/parameter requirement	+	−	−	+	−
Compensation for VSI nonlinearity	+	+	−	−	+
Compensation for R_s variation	+	−	−	−	+
Compensation for cross-coupling	+	+	−	−	−
Applicability over wide speed range	+	+	−	+	−
Additional loss, noise, EMI, etc…	+	+	+	−	+
Individual PM Temperature Info.	+	−	−	−	+
Detection of rotor asymmetry	−	−	−	−	+
Robustness to abnormal cooling	+	−	+	+	+

an expression for Λ_{PM} can be derived from (2)-(3) as

$$\Lambda_{PM}^r = \{V_{qs}^r - R_s I_{qs}^r - \Omega_r L_{ds}(I_{qs}^r, I_{ds}^r)I_{ds}^r\}/\Omega_r, \qquad (4)$$

from which T_{PM} can be calculated from the terminal quantities, V_{qs}, I_{qs}, and Ω_r, and parameters, R_s and L_{ds}, from (1).

Although estimation of T_{PM} from Λ_{PM} appears to be straightforward with all the variables and parameters in (1) and (4) available, there are a number of non-idealities to be considered. The existing work on model or signal injection based T_{PM} estimation show that compensation for the following is required to avoid excessive error in the T_{PM} estimate [17]-[24].

1) Temperature dependency of R_s: R_s increases with stator winding temperature at 0.393%/°C.

2) Inverter non-linearity: there is a discrepancy between the reference and actual stator input voltage, V_{qs}, due to dead-time and voltage drop in the inverter components [25].

3) Inductance variation: the value of L_{ds} varies with saturation and cross coupling between the d- and q-axes, and T_{PM} [19], [25]-[27]

It is possible to compensate for the variation in R_s and inverter non-linearity with a model or additional measurements of stator temperature or voltage [17], [20]-[22], or these non-ideal effects can be avoided [18]-[21]. However, this results in increased complexity of T_{PM} estimation, and adds cost and/or computational requirements, which could be a limiting factor in industrial drives.

Although a deterministic approach can be applied to take R_s variation and inverter non-linearity into account, the L_{ds} behavior under saturation, cross coupling, and temperature variation is difficult to model. This makes it difficult to fully cancel the effects through modelling or a compensation algorithm. The error in the T_{PM} estimate due to L_{ds} variation is usually minimized with an inductance map or look up table

(LUT) that is predetermined from a series of tests, where L_{ds} is obtained from I_{qs} and I_{ds} [17]-[24]. It is not possible to avoid the use of a LUT, if electrical model or parameters are involved due to the nature of the flux distribution and non-ideal inductance variation in actual PMSMs. Although the error cannot be eliminated, the results in [17]-[24] show that the precision in the T_{PM} estimates obtained using a predetermined LUT is sufficient for thermal protection purposes.

III. Airgap Flux Search Coil Based Estimation of T_{PM} for PM Thermal Monitoring

A. Search Coil-based T_{PM} Estimation

If the airgap flux measurement is available in the PMSM for control or fault detection purposes, T_{PM} monitoring based on Λ_{PM} estimation can be simplified from the model-based method described in section II. It is also possible to install a low-cost search coil around a stator tooth to include fault monitoring and/or T_{PM} monitoring features to the drive system. Since the local airgap flux linkage can be directly measured with a search coil, estimation of Λ_{PM} does not involve temperature dependent resistance parameters or inverter non-linearity. The search coil voltage, e_{sc}, is independent of inverter non-idealities since it is directly measured. In addition, the current flow through the search coil is negligible due to the high input impedance of the measurement system making it independent of search coil resistance. This eliminates the need for the first 2 items listed in section II that require compensation, which simplifies Λ_{PM} based thermal monitoring compared to that of thermal/electrical model or signal injection-based methods.

The stator as, bs, cs and rotor d, q magnetic axes are shown in Fig. 1, where θ_r is the angle between the as and q axes. If a single search coil is installed in the stator, θ_{sc} apart from the as axis, the magnetic axis of the search coil, sc, can be represented as shown in Fig. 1. The d and q axis search coil voltages, e_{qsc}, e_{dsc}, in the rotor reference frame can be calculated from the e_{sc} measurement since θ_r and θ_{sc} are known. Considering that the search coil voltage is independent of its resistive component and behaves as the secondary of a step-down transformer, analytic equations for e_{qsc} and e_{dsc} can be derived from (2) as

$$e^r_{qsc} = \frac{N_{sc}}{N_s}(p\lambda^r_{qs} + \omega_r \lambda^r_{ds}) = a \cdot (p\lambda^r_{qs} + \omega_r \lambda^r_{ds}),$$
$$e^r_{dsc} = \frac{N_{sc}}{N_s}(p\lambda^r_{ds} - \omega_r \lambda^r_{qs}) = a \cdot (p\lambda^r_{ds} - \omega_r \lambda^r_{qs}), \quad (5)$$

where $N_{sc}/N_s = a$ is the effective turns ratio between the search coil and stator winding. From (3) and (5), the search coil voltage can be simplified to

$$E^r_{qsc} = a\Omega_r \Lambda^r_{ds} = a\Omega_r(L_{ds}(I^r_{qs}, I^r_{ds}) \cdot I^r_{ds} + \Lambda^r_{PM}),$$
$$E^r_{dsc} = -a\Omega_r \Lambda^r_{qs} = a\Omega_r(L_{qs}(I^r_{qs}, I^r_{ds}) \cdot I^r_{qs}), \quad (6)$$

in *steady state*.

The information regarding the PM flux linkage is included only in the E_{qs} or Λ_{ds} components. An expression for the Λ_{ds} component of the search coil, Λ_{dsc}, can be derived from (6) as

$$\Lambda^r_{dsc}(I^r_{qs}, I^r_{ds}, T) = a\Lambda^r_{ds} = E^r_{qsc}/\Omega_r$$
$$= a(L_{ds}(I^r_{qs}, I^r_{ds}) \cdot I^r_{ds} + \Lambda^r_{PM}), \quad (7)$$

and the measurement of Λ_{dsc} at reference temperature (T_0), Λ_{dsc0}, can be expressed as

$$\Lambda^r_{dsc0}(I^r_{qs}, I^r_{ds}, T_0) = a(L_{ds}(I^r_{qs}, I^r_{ds}) \cdot I^r_{ds} + \Lambda^r_{PM0}). \quad (8)$$

The relationship between the change in Λ_{dsc}, $\Delta\Lambda_{dsc}$, due to T_{PM} variation can be derived by subtracting (8) from (7) as

$$\Delta\Lambda^r_{dsc} = \Lambda^r_{dsc}(I^r_{qs}, I^r_{ds}, T) - \Lambda^r_{dsc0}(I^r_{qs}, I^r_{ds}, T_0)$$
$$= a(\Lambda^r_{PM} - \Lambda^r_{PM0}) = \Lambda^r_{PMsc} - \Lambda^r_{PMsc0}, \quad (9)$$

where it is assumed that the error due to the temperature dependence of L_{ds} is not substantial for thermal protection purposes.

From (1) and (9), the equation for estimating T_{PM} can be derived as

$$T_{PM} = T_0 + \frac{\{\Lambda^r_{dsc}(I^r_{qs}, I^r_{ds}, T) - \Lambda^r_{dsc0}(I^r_{qs}, I^r_{ds}, T_0)\}}{\alpha \cdot \Lambda^r_{PMsc0}}. \quad (10)$$

This equation shows that T_{PM} can be estimated from the Λ_{ds} (E_{qs}) estimate, PM temperature coefficient, α, search coil measurement of Λ_{PMsc} and Λ_{dsc} at reference temperature T_0, Λ_{PMsc0} and Λ_{dsc0}, which are all known parameters and variables. The values of Λ_{dsc0} can be stored as a function of I_{qs} and I_{ds} as an equation or a LUT to compensate for the non-ideal magnetic saturation and cross coupling.

B. Implementation of Proposed T_{PM} Estimation Method

The block diagram for implementing the proposed airgap flux search coil-based T_{PM} estimation method is shown in Fig. 2. It is assumed that the stator currents, i_{as}, i_{bs}, and i_{cs}, and rotor position, θ_r, are available in addition to the search coil voltage, e_{sc}, measurement. A 2 dimensional finite element (FE) analysis was performed on the PMSM tested in section V for designing the suitable filters and to observe the influence of the non-ideal variation in L_{ds} characteristics with temperature. The FE model of the 12 pole, 2.2 kW IPMSM test motor is shown in Fig. 3(a) with the search coil placed to enclose the tooth of one stator slot. The magnetic axis of the search coil is in-line with that of phase a of the stator ($\theta_{sc}=0^o$) in the FE model.

The key variable Λ_{dsc} that holds the information on Λ_{PM} (and T_{PM}), is calculated from the q-axis component of the search coil voltage, E_{qsc}, and speed, Ω_r, from (7). To remove the switching frequency components in the search coil voltage,
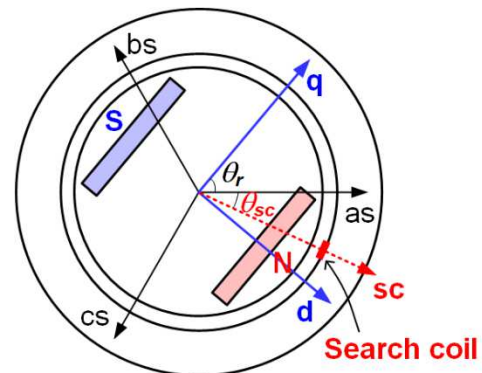

Fig 1. Representation of stator as, bs, cs, rotor d, q magnetic axes, and the search coil magnetic axis, sc, in a 2 dimensional plane with θ_r and θ_{sc} shown.

e_{sc}, an analog low pass filter is applied to e_{sc} to obtain $e_{sc,LPF}$. The low pass filtered search coil voltage $e_{sc,LPF}$ is also rich in space harmonics that are odd integer multiples of the fundamental speed frequency due to the narrow span of the search coil, as shown in Fig. 3(b). Since harmonic components interfere with the computation of E_{qsc}, they must also be filtered out to prevent estimation errors. The low pass filtered e_{sc} signal is bandpass filtered, $e_{sc,BPF}$, to extract only the fundamental speed frequency. Considering variable speed operation, the passband is synchronized to the rotor speed. E_{qsc} can be obtained from the $e_{sc,BPF}$ signal, rotor and search coil position, θ_r, θ_{sc}, to calculate Λ_{dsc}. The change in the magnitude and phase angle of $e_{sc,BPF}$ due to filtering is compensated for from the frequency dependent filter response to avoid distortion in the Λ_{dsc} estimate. The processing of e_{sc} required for estimation of Λ_{dsc} is summarized in Fig. 2.

Once the estimate of Λ_{dsc} at a given I_{qs} and I_{ds} is available, the change with respect to its value at T_0 (Λ_{dsc0}), $\Delta\Lambda_{dsc}$, is required for calculation of T_{PM} from (10). To take the non-ideal influence of core saturation and cross coupling on the value of L_{ds} into account, the values of Λ_{dsc0} were measured and stored as a 2 dimensional LUT under the operating range of the motor as a function I_{qs} and I_{ds}. $\Delta\Lambda_{dsc}$ can be calculated from the Λ_{dsc} estimate and Λ_{dsc0} obtained from the LUT at the present values of I_{qs} and I_{ds} to calculate T_{PM}. The value of Λ_{PMsc0} is obtained from the Λ_{dsc} estimate obtained under no load condition.

It was also shown in a number of resources that L_{ds} is also dependent on T_{PM}, which could lead to estimation errors [13], [19]. The results of the FE analysis showing the expected error in the T_{PM} estimate due to L_{ds} variation at 60ºC above T_0 as a function of I_{qs} and I_{ds} is given in Fig. 4 for the test motor. It can be seen that the error is below 0.4ºC when operating below rated current. Although there are ways of reducing the errors based on additional compensation, it was not pursued in this work considering that the purpose of T_{PM} estimation is for thermal protection. The intention was to keep the method for PM thermal protection simple, as shown in Fig. 2.

C. Additional Benefits of Airgap Search Coil based Thermal Monitoring

If the search coil measurement of the local airgap flux is available, the flux from the individual PMs can be measured. This makes it possible to extract useful information from the e_{sc} measurements in addition to average PM temperature, such as asymmetry in the rotor due to rotor faults and non-uniform T_{PM} of individual PMs. The PM temperature estimate obtained from model- or signal injection-based methods represent the "average" T_{PM}. This is because the PM is usually represented as one component of the thermal model, and the back-emf voltage or the injected signal represents that from the average of all poles considering the stator winding structure. Therefore, it is possible to obtain the "maximum" T_{PM} estimate from the individual poles with minimum Λ_{dsc} or E_{qsc} values. This provides improved thermal protection based on the maximum T_{PM} rather than the average T_{PM}, in case of the temperature distribution of PM between poles is non-uniform [28]. This can occur due to part-to-part variance between the PMs or other non-idealities or manufacturing imperfections in the PMSM rotor such as magnetic anisotropy, shorted laminations, etc.

Another advantage of having an airgap flux search coil is its sensitive and reliable fault detection capability [5]-[7]. Detection of faults in the PMSM with conventional vibration or current spectrum analysis is a non-trivial task since all faults PMSM rotor, coupling, or load produce identical rotor speed-related fault frequency components in the current or vibration spectra. This makes it difficult to distinguish the source of the
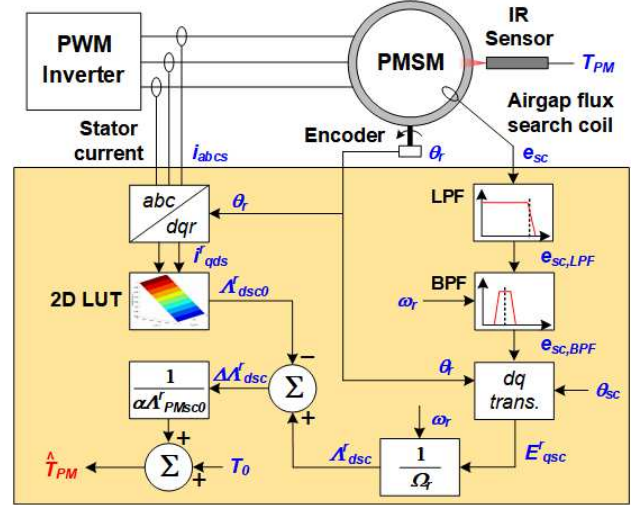

Fig 2. Block diagram representation of proposed airgap flux search coil-based T_{PM} estimation method

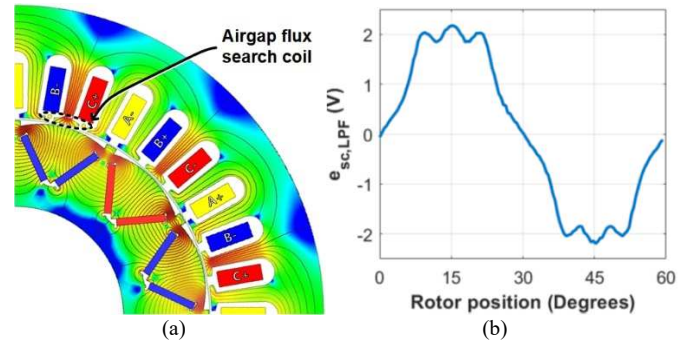(a)   (b)

Fig 3. (a) 2 dimensional FE analysis model of 12 pole, 2.2 kW IPMSM used for experimental verification; (b) simulation results of e_{sc} waveform, $e_{sc,LPF}$, after low-pass filtering of switching frequency components and before band-pass filtering of fundamental frequency component.
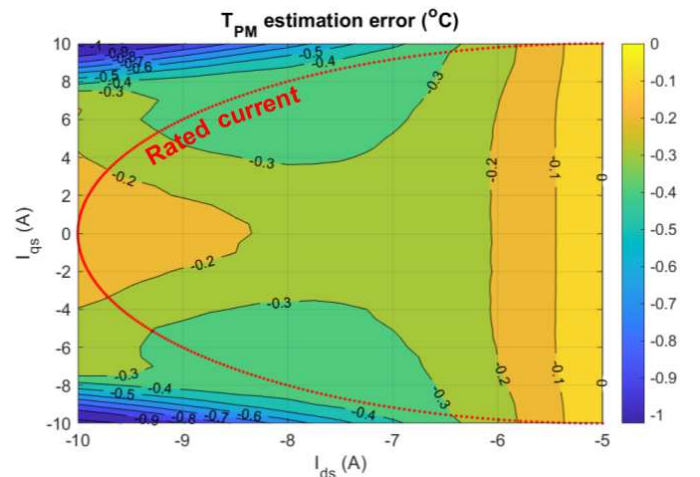

Fig. 4. FEA results of temperature estimation error due to d-axis inductance variation when T_{PM} is 60ºC above T_0.

problem. There are other problems with current spectrum analysis such as the observability of PMSM faults depending on the speed or current controller parameter and motor topology making fault detectability unpredictable. In addition, the conventional Fourier transform-based techniques cannot be applied under variable speed conditions common in PMSM applications. Time-frequency transformation methods are required as a solution, which complicates the method. It is shown in [7] that the problems listed above can be solved with airgap flux search coil monitoring since the flux of each individual pole is measured directly.

When the PMs are identical, the magneto-motive force (MMF) of the PMs and the positive (N) and negative (S) peaks of e_{sc} are identical as shown in the FE results of $e_{sc,BPF}$ in Fig. 5(a)-(b). However, if one of the PMs is operating at higher temperature or is demagnetized, the MMF of that pole decreases as shown in Fig. 5(a). In this case, one of the N or S pole peaks in Λ_{sc} (or E_{sc}) decrease as a result of the decrease in one of the MMF peaks, as shown in the FE results of $e_{sc,BPF}$ given in Fig. 5(c). This shows that the airgap search coil enables monitoring of the T_{PM} of the individual PMs, and therefore, can provide thermal protection based on the T_{PM} of the hottest PM. This was not possible with model or signal injection based methods that can only provide an estimate of the average T_{PM} of all PMs. The back emf voltage measured for the case of Fig. 6(b) with one demagnetized PM is shown in Fig. 5(d). This shows that the asymmetry in the PMs is not observable with the motor model since the stator windings span the PMs of all poles (similar for signal injection methods).

IV. EXPERIMENTAL RESULTS

A. Experimental Setup

The proposed method was verified on a 2.2 kW, 12 pole IPMSM shown in Fig. 6, where the ratings are shown in Table II. The test motor was controlled with a commercial inverter and loaded with an identical PMSM of the same rating, as shown in Fig. 6(a). The test motor was covered with a thermal insulator to maximize the temperature increase within rated operating conditions. To evaluate the accuracy of the T_{PM} estimate, an infrared (IR) sensor was installed on the non-drive end for non-contact measurement of PM temperature. The IR sensor was installed through a hole drilled in the end shield, as shown in Fig. 6(b). The end plate of the rotor on the non-drive end was removed, and a special black paint coating with high emissivity was applied to the surface, as shown in Fig. 6(c), to improve the measurement accuracy. The sensor was placed to measure the temperature that best represents the average temperature of rotor surface and PM of the region highlighted in Fig. 6(d). Although the temperature measurement is not the temperature of the PMs, it is expected to be close to the actual T_{PM} under thermal equilibrium.

To test under the condition where the temperature of the

Table II. Ratings and design of IPMSM test motor

P_{Rated} (kW)	V_{rated} (V)	I_{rated} (A)	N_{rated} (rpm)	# of poles	Slots
2.2	144	9.6	1750	12	36

(a)

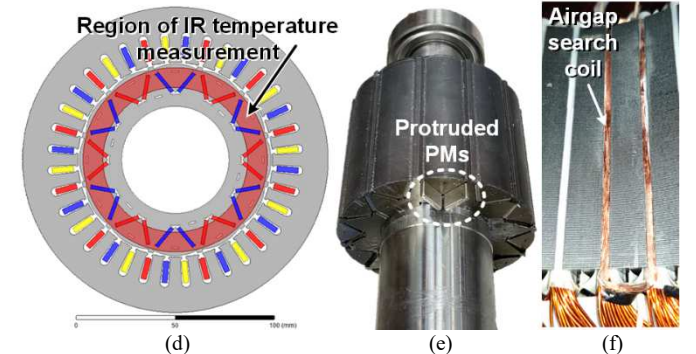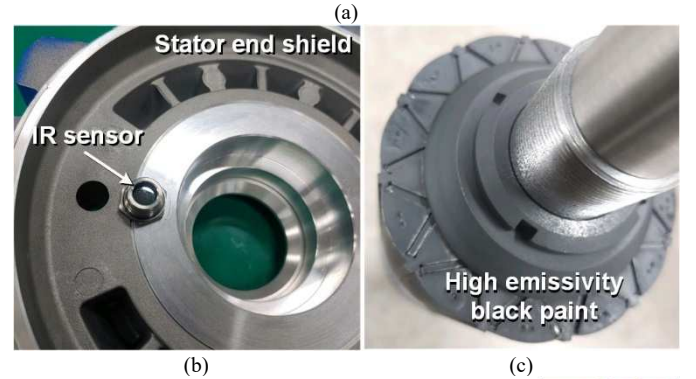(b)   (c)

(d)   (e)   (f)

Fig 6. Experimental test setup: (a) test motor and load; (b) IR sensor installed in stator end shield; (c) rotor surface with high emissivity paint; (d) region of average IR temperature measurement; (e) protruded PMs for emulating local temperature rise or local demagnetization; (f) 5 turn airgap flux search coil.
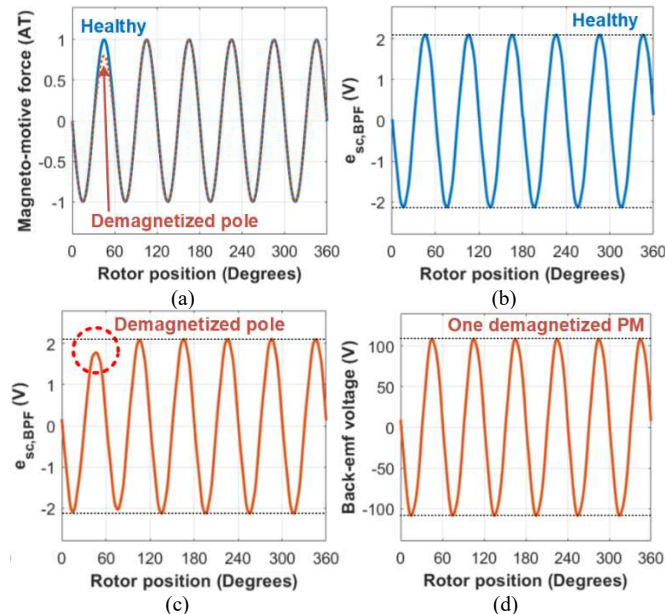

Fig 5. FE analysis results of expected MMF, $e_{sc,BPF}$, and back EMF voltage waveforms for healthy rotor ((a)-(b)), rotor with one demagnetized pole due to non-uniform T_{PM} distribution or demagnetization ((a),(c),(d)).

PMs are not uniform and/or partial demagnetization, the PMs of one pole was pushed out by 10% of the PM axial length on the drive end, as shown in Fig. 6(e). The protruded PMs result in a decrease in the flux of one pole, which emulates increase in the local PM temperature or local demagnetization. The airgap flux was measured with a 5 turn search coil installed around a single stator tooth, as shown in Fig. 6(f). For the test motor, the magnetic axis of the search coil was aligned to that of stator phase A ($\theta_{sc}=0$), as shown in Fig. 3(a). The band pass filtered v_{as} and e_{sc} measurements along with rotor angle, θ_r, obtained from the encoder, shown in Fig. 7, confirm that the search coil installation and filter operation are correct. T_{PM} estimation was performed from the measurements of e_{sc}, θ_r, i_{abcs} and predetermined and stored parameters and variables Λ_{dsc0}, Λ_{PMsc0}, α, and T_0, as summarized in Fig. 2.

B. Experimental Results

The values of the stator current, I_{qs}, I_{ds}, rotor speed, N_m, T_{PM} estimate and IR sensor measurement, and the T_{PM} estimation error are shown in Fig. 8. The T_{PM} estimate was compared to the IR sensor measurement with the motor operated continuously for 5.25 hours (315 minutes) under varying speed and load conditions. The test motor was run with the load varied between 5 % and 70 % rated load, and with the speed varied between 400 rpm and rated speed of 1750 rpm to cover a wide operating range. The IR sensor measurement of the PM was increased from 20°C to 65°C to keep the temperature of the IR sensor within the specified ambient temperature limit of 50°C. The load was varied at mostly above 50% rated load up to 150 minutes of operation to observe how the proposed method tracks the increase in PM temperature. The motor was gradually cooled down after 150 minutes up to 250 minutes by maintaining the load below 50% rated load. The load was increased and decreased again between 250 and 315 minutes under varying speed and load conditions, to test the performance of the proposed method. The estimate of T_{PM} was obtained once every 25 seconds considering that the thermal time constant is large, and the purpose is for thermal protection.

The results of Fig. 8 show that the T_{PM} estimate is capable of tracking the change in PM temperature. It can be seen that the noise level of the T_{PM} estimate is relatively high when the rotor speed is low. This can be attributed to the magnitude of the induced search coil voltage being proportional to the rotor speed. It is possible to low pass filter the T_{PM} estimates to reduce the error and noise level; however, this will introduce a delay in T_{PM} estimation. The relatively higher error during low-speed operation can be tolerated when T_{PM} is used for thermal protection, since T_{PM} is more likely to exceed the thermal limit under high speed operation when the eddy current losses in the PM are higher [14].

It can be seen in Fig. 8 that the error between the T_{PM} estimate and IR sensor measurement is largest during initial operation and low speed between 0 and 15 minutes. This is due to the combination of the low search coil voltage at low speed (400 rpm), and the discrepancy between the actual T_{PM} and IR measurement. In a PMSM, the temperature of the PM is higher than that of the rotor core mainly due to the higher eddy current losses in the PM produced by the harmonics in the flux [22].

Therefore, when the motor at ambient temperature is initially accelerated from standstill, the temperature of the PM increases rapidly starting at the center of the PM. The temperature distribution within the PM becomes uniform with thermal conduction, and then the heat from the PM gradually conducts to the rotor core with a non-negligible thermal time constant. Considering that the IR sensor is measuring the average temperature of the PM and rotor core at the axial end surface, the rise in the IR measurement is expected to be slower than that of the PM. Therefore, the actual T_{PM} is expected to be higher than the IR sensor measurement shown in Fig. 8 making the actual T_{PM} estimation error smaller. Considering the arguments above, the proposed method is expected to provide estimation of T_{PM} sufficient for thermal monitoring purposes.

The waveform of the band-pass filtered measurements of e_{sc} and v_{as} are shown in Fig. 9(a)-(b), respectively, with the PMs in one of the poles protruded by 10%, as shown in Fig. 6(e). There was a 7.7% decrease in one of the 12 $e_{sc,BPF}$ peaks from 3.115 V to 2.875 V due to the reduced PM flux, as can be clearly seen in the $e_{sc,BPF}$ waveform. This shows that it is possible to detect the decrease in flux of the individual PMs, if
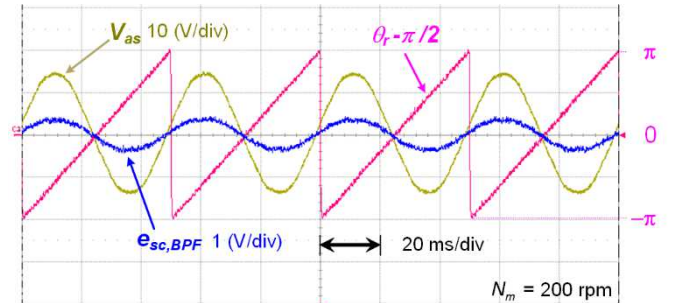

Fig 7. Experimental results: band pass filtered measurements of v_{as}, e_{sc}, and θ_r with $\theta_{sc}=0$.
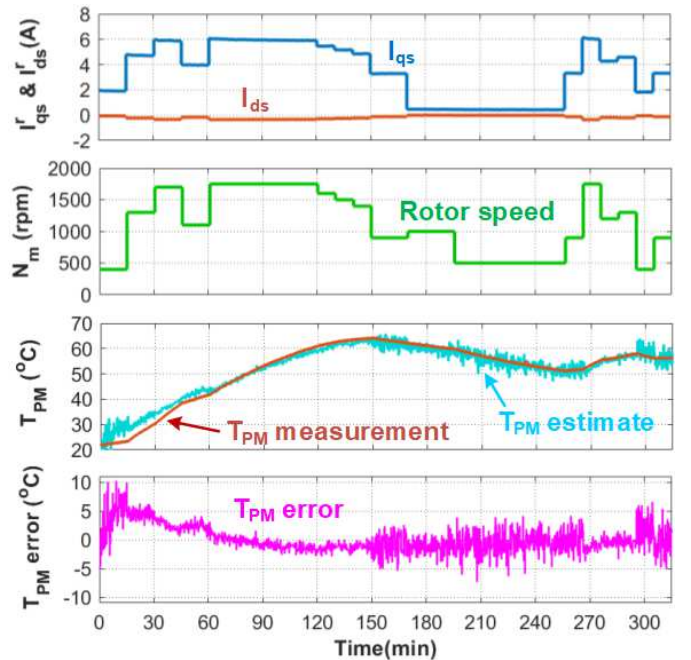

Fig 8. Experimental results of proposed T_{PM} estimation method: Stator current, I_{qs} and I_{ds} (1st row); rotor speed, N_m (2nd row); estimate and measurement of T_{PM} (3rd row); T_{PM} estimation error (4th row).
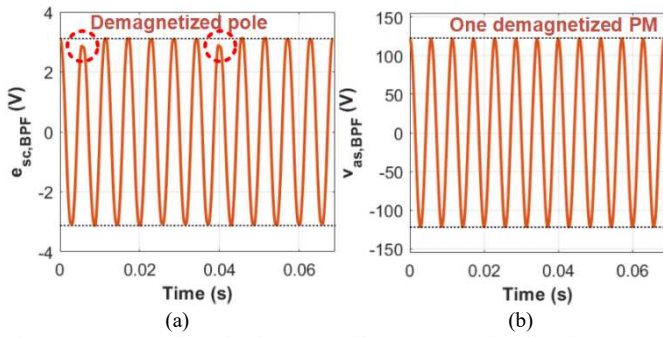
Fig 9. Experimental results: band pass-filtered (a) search coil voltage, $e_{sc,BPF}$, and (b) phase a voltage, v_{as}, waveform with PMs protruded in one pole of rotor (Fig. 7(e)).

caused by non-uniform T_{PM} distribution, which allows the maximum temperature to be monitored for thermal protection. This is expected to provide improved thermal protection over model or signal injection-based methods that provide the average T_{PM} estimate. The stator voltage, v_{as}, representative of the back-emf voltage shows that the asymmetry in the PMs cannot be observed with model-based methods for which the stator windings span the PMs of all poles (similar for signal injection methods). This also shows that asymmetry in the rotor PMs due to local demagnetization can also be detected if the proposed search coil based T_{PM} estimation is used.

V. Conclusion

The feasibility of using the airgap flux search coil voltage measurement for T_{PM} estimation was evaluated in this paper. A new method was proposed and verified through experimental testing. It was shown that existing T_{PM} estimation methods based on thermal/electrical model or signal injection can be simplified with the proposed method, since compensation for stator winding resistance or inverter non-linearity are not required. It was also shown that the proposed method can provide an estimate of the temperature of individual PMs, since the flux of individual PMs can be measured with a search coil with narrow coil span. This allows thermal protection to be performed based on the T_{PM} of the hottest PM and not the average of the PMs. Experimental test results performed under varying speed and load conditions showed that the proposed method can provide T_{PM} estimates with sufficient precision for thermal protection. It was also shown that asymmetry in the rotor due to local demagnetization can be detected. The proposed thermal protection method can be implemented with a single airgap search coil. A low-cost search coil in the stator is expected to help provide advanced thermal protection and fault detection for improving the reliability of the PMSM drive system.

References

[1] "ABB Ability Smart Sensor for motors," 2018, [online] Available: https://new.abb.com/motors-generators/service/advanced-services/smart-sensor/ smart-sensor-for-motors.

[2] "WEG Motor Scan – Whitepaper," [online] Available: https://www.weg.net/wegmotorscan/en/downloads.

[3] S.B. Lee et al., "Condition monitoring of industrial electric machines: state of the art and future challenges," *IEEE Ind. Electron. Mag.*, vol. 14, no. 4, pp. 158-167, Dec. 2020, doi: 10.1109/MIE.2020.3016138.

[4] J. Shin, Y. Park, S. Lee, "Flux-based detection and classification of induction motor eccentricity, rotor cage, and load defects," *IEEE Trans. Ind. Appl.*, vol. 57, no. 3, pp. 2471-2480, May/Jun. 2021.

[5] Y. Da, X. Shi, M. Krishnamurthy, "A new approach to fault diagnostics for permanent magnet synchronous machines using electromagnetic signature analysis," *IEEE Trans. Power Electron.*, vol. 28, no. 8, pp. 4104-4112, Aug. 2013.

[6] K. Kang, J. Song, C. Kang, S. Sung, G. Jang, "Real-time detection of the dynamic eccentricity in permanent-magnet synchronous motors by monitoring speed and back EMF induced in an additional winding," *IEEE Trans. Ind. Electron.*, vol. 64, no. 9, pp. 7191-7200, Sept. 2017.

[7] M. S. S. Rafaq et al., "Airgap search coil based identification of PM synchronous motor defects," *IEEE Trans. Ind. Electron.*, Early Access, doi: 10.1109/TIE.2021.3095810.

[8] G. C. Stone, I. Culbert, E. A. Boulter, H. Dhirani, *Electrical insulation for rotating machines-design, evaluation, aging, testing and repair*, Hoboken, NJ, USA, Wiley-IEEE Press, 2014.

[9] Y. Park, S. B. Lee, J. Yun, M. Sasic, G. C. Stone, "Air gap flux-based detection and classification of damper bar and field winding faults in salient pole synchronous motors," *IEEE Trans. Ind. Appl.*, vol. 56, no. 4, pp. 3506-3515, July/Aug. 2020, doi: 10.1109/TIA.2020.2983902.

[10] Y. Da, X. Shi, M. Krishnamurthy, "A novel universal sensor concept for survivable PMSM drives," *IEEE Trans. Power Electron.*, vol. 28, no. 12, pp. 5630-5638, Dec. 2013.

[11] Y. Kwon, S. Sul, N. A. Baloch, S. Morimoto, M. Ohto, "Design, modeling, and control of an IPMSM with an asymmetric rotor and search coils for absolute position sensorless drive," *IEEE Trans. Ind. Appl.*, vol. 52, no. 5, pp. 3839-3850, Sept./Oct. 2016.

[12] J.R. Hendershot, T.J.E. Miller, *Design of brushless permanent magnet motors*, Oxford Science Publications, USA, 1994.

[13] S. Li, B. Sarlioglu, S. Jurkovic, N. R. Patel, and P. Savagian, "Analysis of temperature effects on performance of interior permanent magnet machines for high variable temperature applications," *IEEE Trans. Ind. Appl.*, vol. 53, no. 5, pp. 4923–4933, 2017.

[14] M Ganchev, C. Kral, T. Wolbank, "Compensation of speed dependency in sensorless rotor temperature estimation for permanent-magnet synchronous motors," *IEEE Trans. on Ind. Appl.*, vol. 49, no. 6, pp. 2487-2495, Nov./Dec. 2013.

[15] B.H. Lee , K.S. Kim , J.W. Jung , J.P. Hong, Y.K. Kim, "Temperature estimation of IPMSM using thermal equivalent circuit," *IEEE Trans. on Magn.*, vol. 48, no. 11, pp. 2949-2952, Nov. 2012.

[16] C. Kral, A. Haumer, S.B. Lee, "A practical thermal model for the estimation of permanent magnet and stator winding temperatures," *IEEE Trans. on Power Electron.*, vol. 29, no. 1, pp. 455-464, Jan. 2014.

[17] O. Wallscheid, A. Specht, J. Bocker, "Observing the permanent-magnet temperature of synchronous motors based on electrical fundamental wave model quantities," *IEEE Trans. Ind. Electron.*, vol. 64, no. 5, pp. 3921–3929, 2017.

[18] G. Feng, C. Lai, W. Li, Z. Li, N. C. Kar, "Efficient permanent magnet temperature modeling and estimation for dual three-phase PMSM considering inverter nonlinearity," *IEEE Trans. Power Electron.*, vol. 35, no. 7, pp. 7328-7340, July 2020.

[19] H.-S. Jung, H. Kim, S.-K. Sul, D. J. Berry, "Magnet temperature estimation of IPMSM by using fundamental reactive energy considering variation of inductances," *IEEE Trans. Power Electron.*, vol. 36, no. 5, pp. 5771–5783, May 2021.

[20] D. Reigosa, D. Fernandez, T. Tanimoto, T. Kato, and F. Briz, "Comparative analysis of BEMF and pulsating HF current injection methods for PM temperature estimation in PMSMs," *IEEE Trans. Power Electron.*, vol. 32, no. 5, pp. 3691–3699, 2017,

[21] D. F. Laborda et al., "Magnet temperature estimation in variable leakage flux permanent magnet synchronous machines using the magnet flux linkage," *Proc. IEEE ECCE*, pp. 6111-6117, 2020.

[22] D. D. Reigosa, F. Briz, P. García, J. M. Guerrero, and M. W. Degner, "Magnet temperature estimation in surface PM machines using high-frequency signal injection," *IEEE Trans. Ind. Appl.*, vol. 46, no. 4, pp. 1468–1475, 2010,

[23] H. Jung, D. Park, H. Kim, S. Sul, D. J. Berry, "Non-Invasive magnet temperature estimation of IPMSM based on high-frequency inductance with a pulsating high-frequency voltage signal injection," *IEEE Trans. Ind. Appl.*, vol. 55, no. 3, pp. 3076-3086, May/June 2019.

[24] D. Reigosa, D. Fernandez, M. Martinez, J. M. Guerrero, A. B. Diez, and F. Briz, "Magnet temperature estimation in permanent magnet synchronous machines using the high frequency inductance," *IEEE Trans. Ind. Appl.*, vol. 55, no. 3, pp. 2750–2757, 2019,

[25] K. Liu, Z. Q. Zhu "Online estimation of the rotor flux linkage and voltage-source inverter nonlinearity in permanent magnet synchronous machine drives," The temperature characteristics of Lds depends on the machine design, and compensation may be required. *IEEE Trans. Power Electron.*, vol. 29, no. 1, pp. 418-427, Jan. 2014.

[26] S. Li, D. Han, and B. Sarlioglu, "Modeling of Interior Permanent Magnet Machine Considering Saturation, Cross Coupling, Spatial Harmonics, and Temperature Effects," *IEEE Trans. Transp. Electrif.*, vol. 3, no. 3, pp. 682–693, 2017.

[27] B. Stumberger, G. Stumberger, D. Dolinar, A. Hamler, M. Trlep, "Evaluation of saturation and cross-magnetization effects in interior permanent-magnet synchronous motor," *IEEE Trans. Ind. Appl.*, vol. 39, no. 5, pp. 1264-1271, Sept./Oct. 2003.

[28] D. Reigosa, D. Fernandez, T. Tanimoto, T. Kato, F. Briz, "Sensitivity analysis of high-frequency signal injection-based temperature estimation methods to machine assembling tolerances," *IEEE Trans. Ind. Appl.*, vol. 52, no. 6, pp. 4798-4805, Nov./Dec. 2016.